JOINT INSTITUTE FOR NUCLEAR RESEARCH
Dzelepov Laboratory of Nuclear Problems

FINAL REPORT ON THE START PROGRAMME

Scintillation detector for measuring the beam profile at the LINAC-200 accelerator

Supervisor:
Uladzimir Kruchonak

Student:
Aleksandr Luzai, Belarus
Gomel State Technical University
Participation period:
July 09 – August 19,
Summer Session 2023

Dubna, 2023

CONTENTS

ABSTRACT

A beam monitoring system consist of two scintillator planes was developed. Each plane consists of 16 2x2x40mm scintillators. This planes are overlapped at a right angle forming 32x32 mm detector area. As a result, the positioning accuracy of the charged particle is 2mm. By using of collimator S-90 β-source the detector profile was calibrated. Automated data collection was implemented by microcontroller.

Introduction

Among the oldest and most common detectors in nuclear physics are scintillators counters, the history of which began in 1919, when α-particles were visually registered in the laboratory of E. Rutherford by light flashes in a ZnS(Ar) crystal. The most important step then In the 1940s. was building L.A. Kubetsky and others. photomultiplier, which made it possible to automatically detect very weak light flashes. In 1947-1948. publications appeared on scintillation counters composed of photomultipliers and crystalline scintillators of organic (naphthalene) and inorganic p - (sodium iodide Nal), which marked the beginning of the intensive development of the scintillation method for recording nuclear radiation. Faster and cheaper organic scintillators based on scintillating liquids also began to be widely used, and starting from the second half of the 1950s. and so far based on scintillating plastics. The properties of scintillators developed in the early period of their development (before 1964) are most fully described in the fundamental monograph by J. Birks [1]. The main field of application of scintillating inorganic crystals at that time was low-energy spectrometry. High energy physics has been dominated by organic scintillation counters, especially plastic ones, which provide higher time resolution and speed. In the early 1960s inorganic scintillators began to be displaced from spectrometric measurements in low-energy physics by the semiconductor detectors that appeared at that time, which surpassed scintillation ones in terms of energy resolution. Inorganic scintillators reappeared in the 1970s, when the need for large-sized spectrometric detectors and multichannel spectrometric setups greatly increased.

With 4π-geometry. At the same time, Nal(T) single crystals were out of competition at first. However, in subsequent years, Cs(TI) single crystals began to be used more and more, especially in combination with solid-state photodetectors. Good results were also obtained with single crystals of non-activated Csl, bismuth germanate (BGO), and barium fluoride (BaF2). Improvement is ongoing characteristics of detectors with the above crystals and their modifications. New promising scintillating materials have appeared, such as lead tungstate (PbWO4), etc. The field of application of detectors based on a large class of inorganic scintillators is very extensive both in scientific and applied

research. The variety of tasks and specific conditions in various physical experiments has a corresponding effect on the design of the detectors used in them. The range of problems solved with the help of plastic scintillators has also significantly expanded. If earlier they were used mainly only in devices for time selection and analysis of events, then in modern installations they are widely used to build detectors for the complete absorption of high-energy radiation - calorimeters, as well as position-sensitive detectors. Liquid organic scintillators are widely used as neutron and neutrino detectors.

Many of the most important results in particle physics have been associated to a large extent with the use of Cherenkov detectors in experiments.
The practical use of Cherenkov radiation, as well as scintillation, began with the advent of photomultipliers. The characteristics of photomultipliers and other photodetectors are being improved constantly in connection with ever-increasing requirements for them, especially dictated by great progress in the development of new scintillation and Cherenkov detectors and their large-scale application in nuclear physics, high energy physics, astrophysics and medicine. Along with vacuum PMTs, solid-state and hybrid photodetectors are increasingly being used in a number of experiments with great success. Particular interest in these devices is manifested in the development of position-sensitive detectors.

Measurement of the characteristics of the 32-channel scintillation counter.

A 32-channel scintillation counter Fig. 1 is considered in the presented work, which is planned to be used as a beam monitor at the LINAC-200 electron accelerator [3].

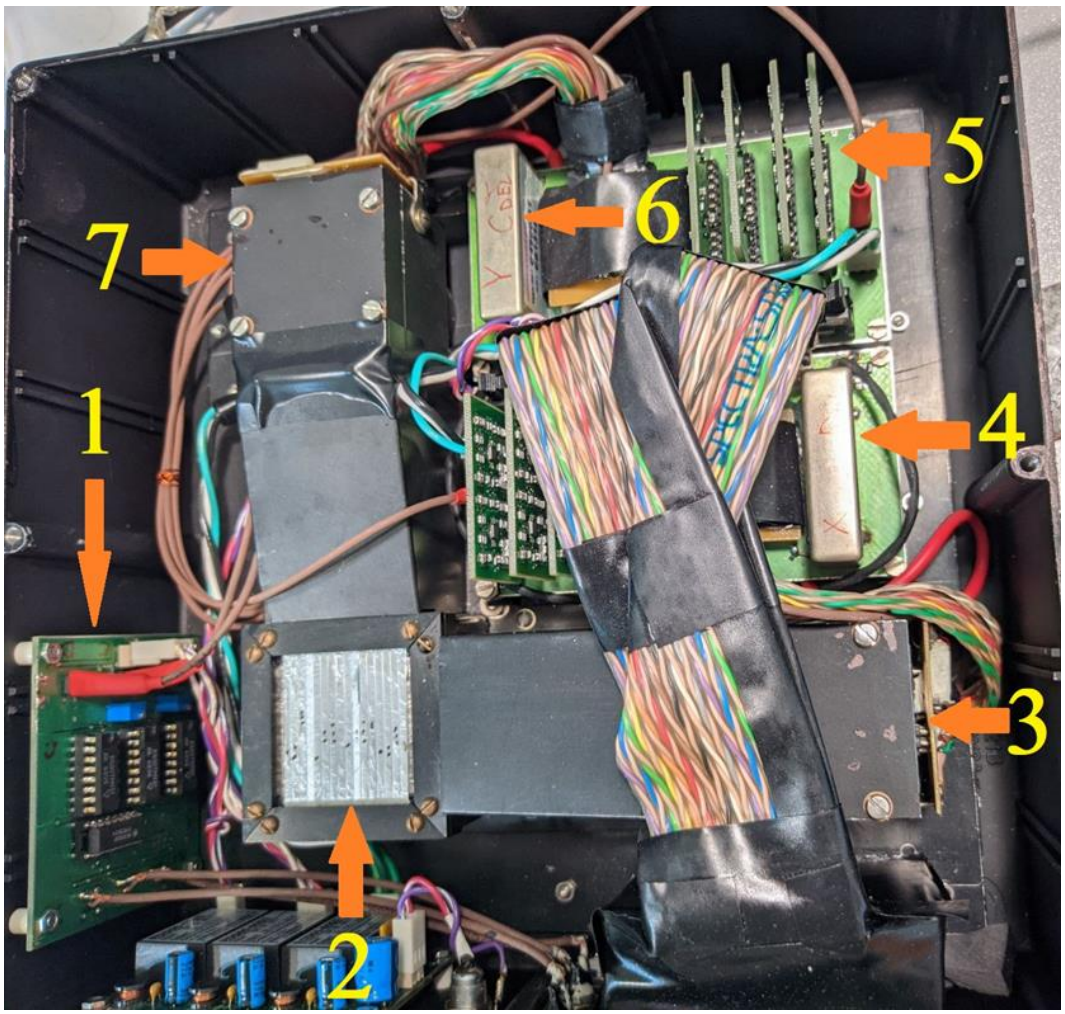

Fig. 1. 32-channel scintillation counter: 1- the scheme of the coincidence signal between the X-planes and Y-planes; 2 -scintillators 3,7 - photomultiplier tubes Hamamatsu H8711 for X-plane and Y-plane; 4,6 - High voltage converters; 5- amplifiers.

For each of the 32 PMTs [4], 20000 PMT amplitude signals were measured using a DRS-4 digital oscilloscope. Recording was performed simultaneously in 4 channels, the trigger input was connected to the coincidence signal between X-plane and Y-plane (look at Fig.2)

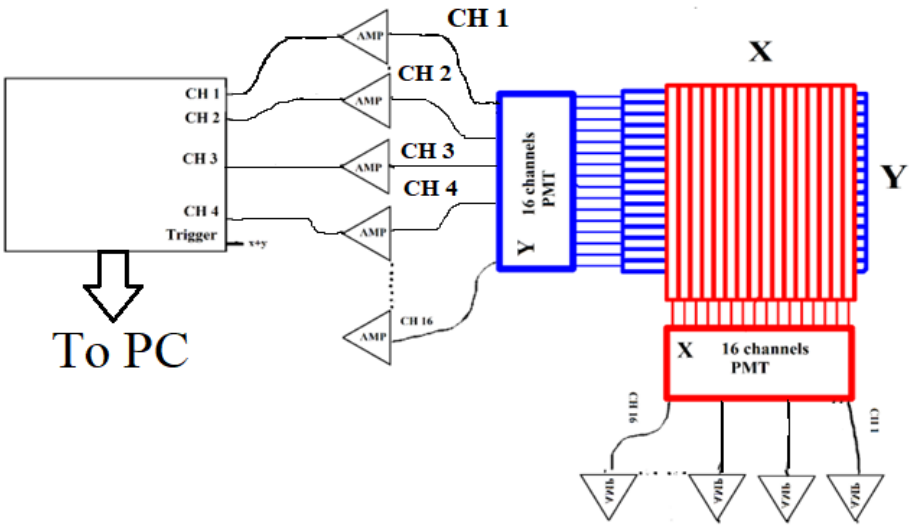

Fig. 2. Oscilloscope connection scheme.

The measured amplitude values were processed using the Gaussian distribution:

$$f(x) = \frac{1}{\sigma\sqrt{2\pi}} e^{-\frac{1}{2}\left(\frac{x-\mu}{\sigma}\right)^2}$$

μ-mean and σ-rms values were computed. The results for the Y-plane are listed in Tab 1 for X-plane are listed in Tab 2 .

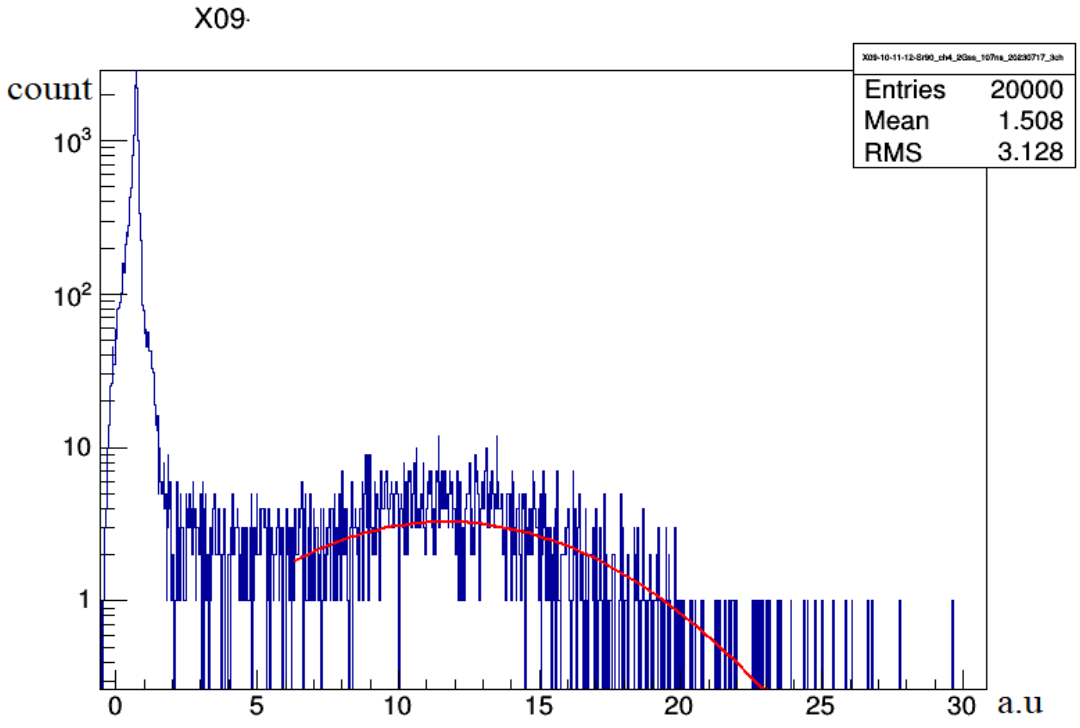

Fig.3. Amplitude spectrum for single scintillator X-9.

№	1	2	3	4	5	6	7	8
Mean	14,2	15,9	15,7	11,5	9,9	6,9	18,1	9
Sigma	4,6	5,5	5,2	3,8	3,6	3,9	6,26	2,9
№	**9**	**10**	**11**	**12**	**13**	**14**	**15**	**16**
Mean	12,4	11,4	12,6	14	13,3	11,6	13,3	11,6
Sigma	4,8	3,7	4,8	5	4,3	4,7	4,3	4,8

Tab.1. Results for Y

The average value of the amplitude for Y is 12,6 arbitrary units.

№	1	2	3	4	5	6	7	8
Mean	5,7	5,66	11,5	10,7	10,4	12,9	14,8	11,8
Sigma	2,08	2,2	3,77	3,4	3,45	4,5	5,1	3,9
№	**9**	**10**	**11**	**12**	**13**	**14**	**15**	**16**
Mean	10,9	12,4	15,3	11,3	9,2	10,8	12,4	10,4
Sigma	4,14	4,7	5	3,9	3,5	4,17	4,17	4

Tab.2. Results for X

The average value of the amplitude for X is 11,01 arbitrary units.

Data acquisition block

Data acquisition block is shown in Fig. 4, it consists of three main parts:

1) The discriminator board is connected to the PMT outputs and converts the analog signal to a discrete signal.
2) 4 8-bit registers based on 74HCT574 chips, where 32 discrete signals from each PMT channel are stored.
3) Reading data from the registers by the ATmega328 microcontroller and transferring it to the computer using USB interface.

The Data acquisition black scheme is given in Appendix 1.

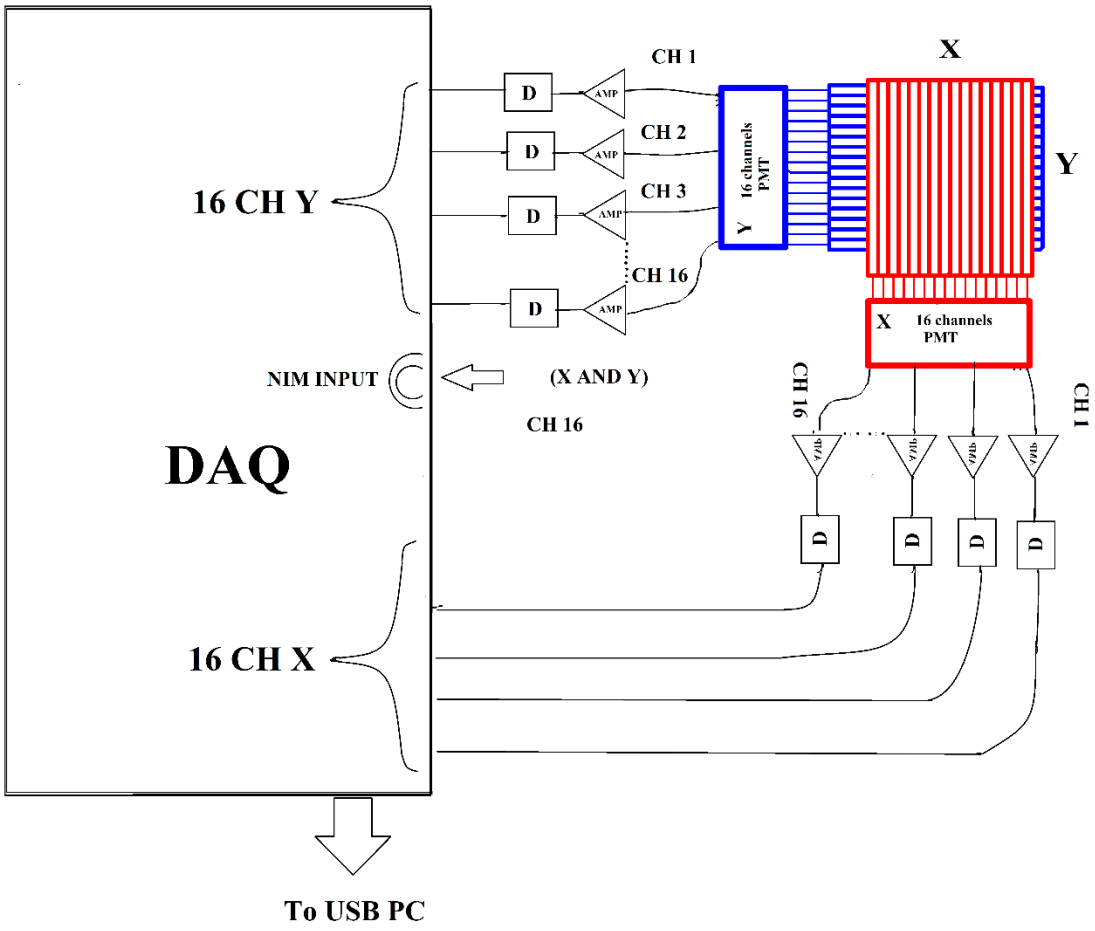

Fig. 4. Data acquisition block scheme.

Writing to the registers occurs on the signal of the coincidence of the X plane with the Y plane. Since the coincidence signal has a NIM standard, i.e. current-based logic, negative "true" (at -16 mA into 50 ohms = -0.8 volts) and 0 mA for "false", and the Data acquisition block was designed on TTL series chips, was developed NIM to TTL converter, its circuit is shown in Fig. 6.

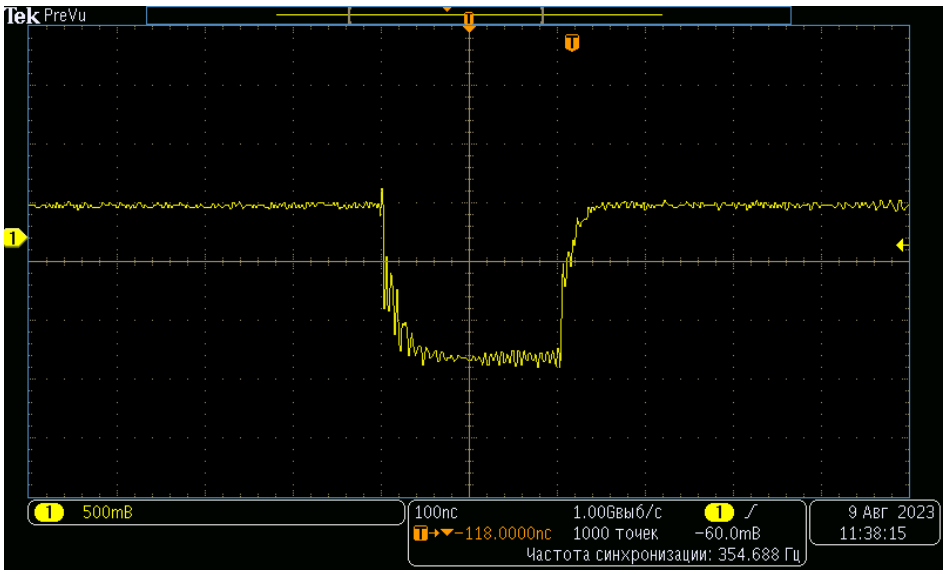

Fig. 5. Coincidence signal (NIM).

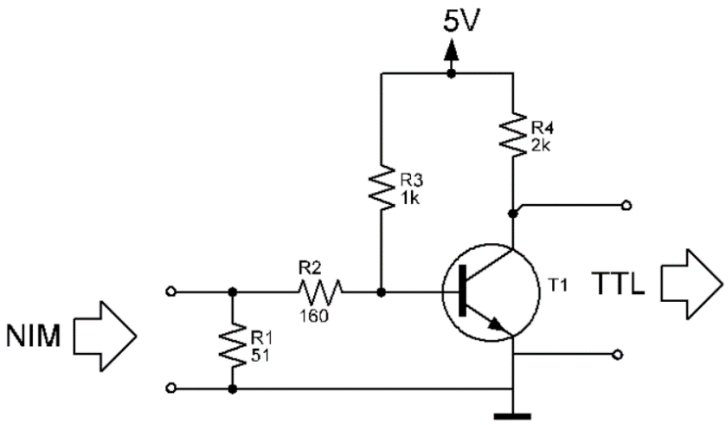

Fig. 6. Scheme of the signal converter from NIM to TTL.

When the circuit input is "false", the transistor is in the open state due to the resistor R3, the resistor R4 is plugged to ground and the output is 0 V. As soon as −0.8 volts is received at the input, the transistor will close and the output will be connected to 5 volts through the resistor R4 . Fig. 7.

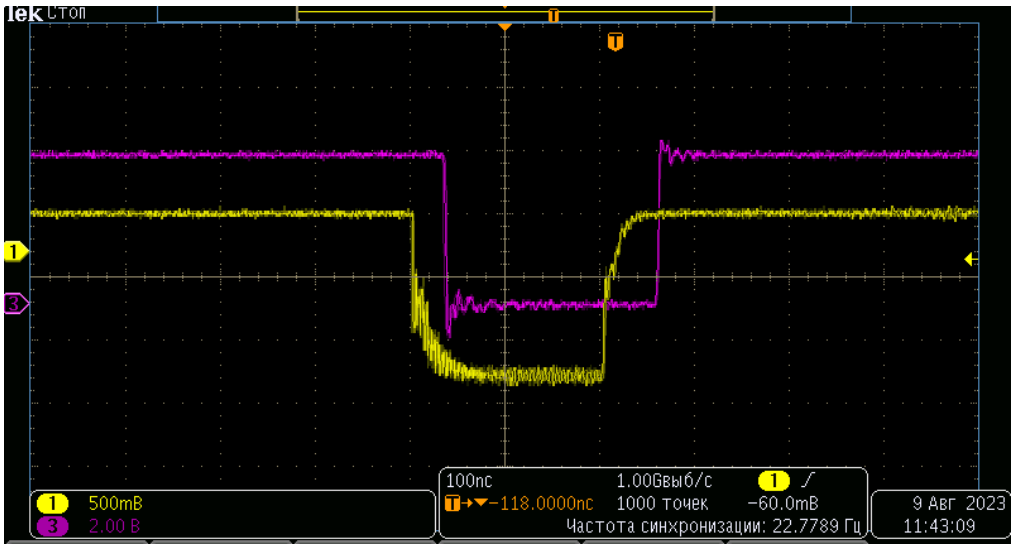

Fig. 7. Converter output. 1- Input signal (NIM). 3 - Output signal (TTL)

The output of the converter is connected to the RS flip-flop, based on two-elements "AND-NOT" (Fig. 8) The RS flip-flop blocks the writing of new data until the microcontroller is calculated.

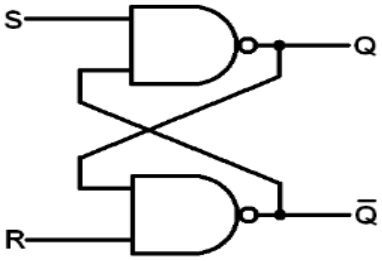

Fig. 8. RS flip-flop.

Table 3. Main parameters of ATmega328 microcontroller[5]:

High Performance, Low Power Atmel®AVR® 8-Bit Microcontroller Family

- Advanced RISC Architecture
  - 131 Powerful Instructions
  - Most Single Clock Cycle Execution
  - 32 x 8 General Purpose Working Registers
  - Fully Static Operation
  - Up to 20 MIPS Throughput at 20MHz
  - On-chip 2-cycle Multiplier
- High Endurance Non-volatile Memory Segments
  - 32KBytes of In-System Self-Programmable Flash program Memory
  - 1KBytes EEPROM
  - 2KBytes Internal SRAM
  - Write/Erase Cycles: 10,000 Flash/100,000 EEPROM
  - Data Retention: 20 years at 85°C/100 years at 25°C(1)
  - Optional Boot Code Section with Independent Lock Bits

As soon as the coincidence signal arrives, the microcontroller goes into interrupt mode, it reads 32 bits information from 4 registers one by one, writes them in buffer and resets the trigger. When the microcontroller is not processing an interrupt, it sends the accumulated in the buffer data to the Serial port.
The SERIAL to USB interface converter is based on the CH340 chip.

The listing of the program for the ATMEGA 328 microcontroller is given in Appendix 2.

Results

In order to visualize the obtained data, a Python program (Appendix 3) was developed using the matplotlib library [6].

The profile was measured using a collimator Sr-90 β-source. The results for 4 different source placement points are presented in Fig. 9-12.

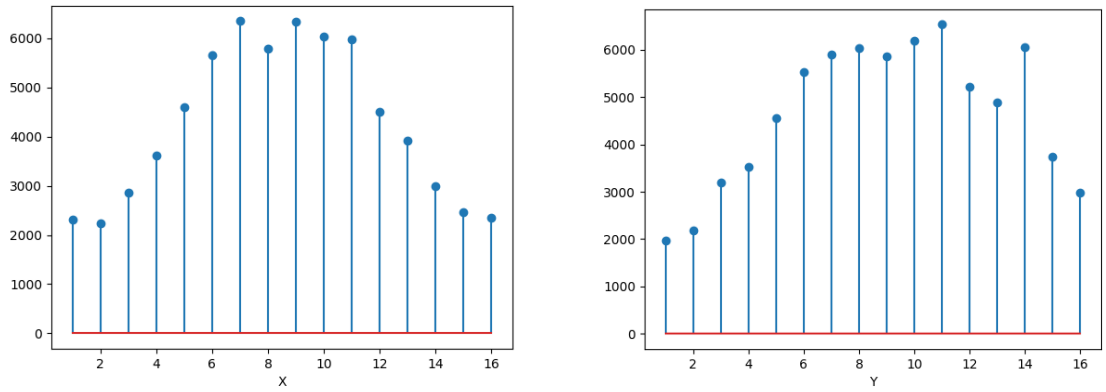

Fig. 9. Counters distribution from Sr90 β -source. The source is located in the center.

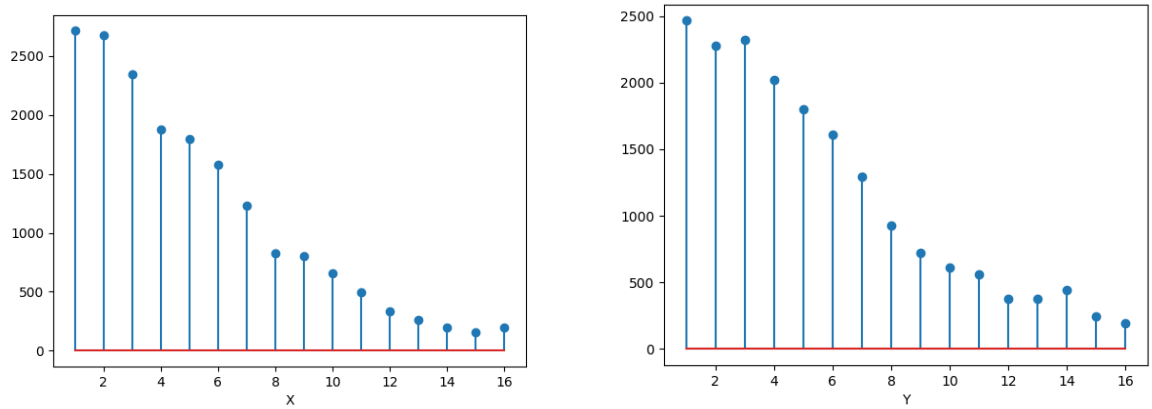

Fig. 10. Counters distribution from Sr90 β -source. The source is located X-0 Y-0.

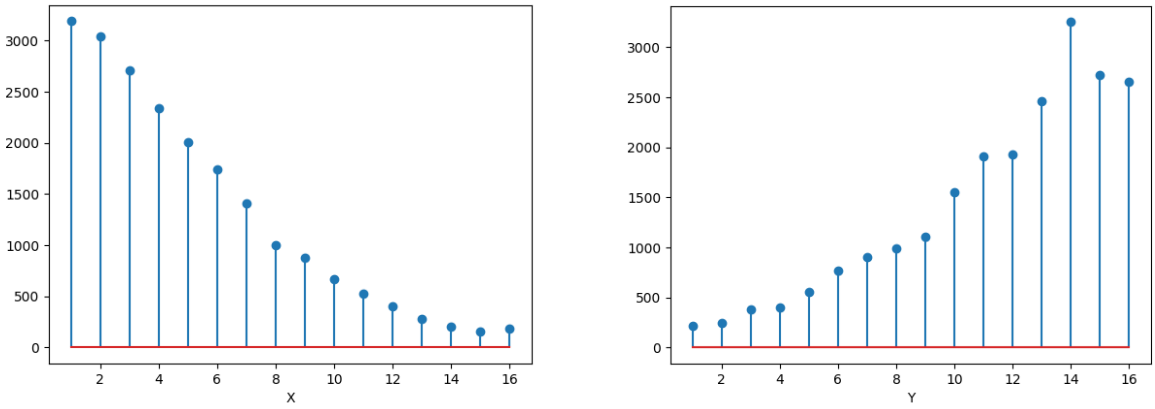

Fig. 11. Counters distribution from Sr90 β -source . The source is located X-0 Y-16.

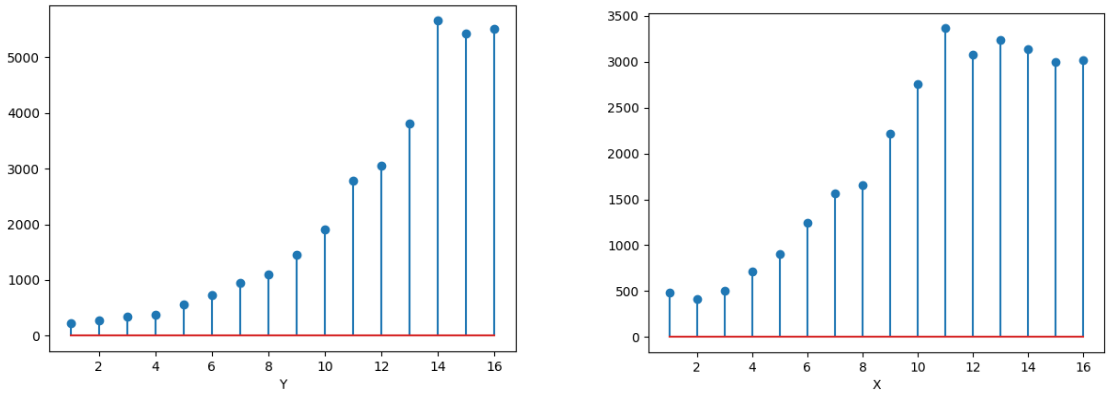

Fig. 12. Counters distribution from Sr90 β -source .The source is located X-16 Y-16.

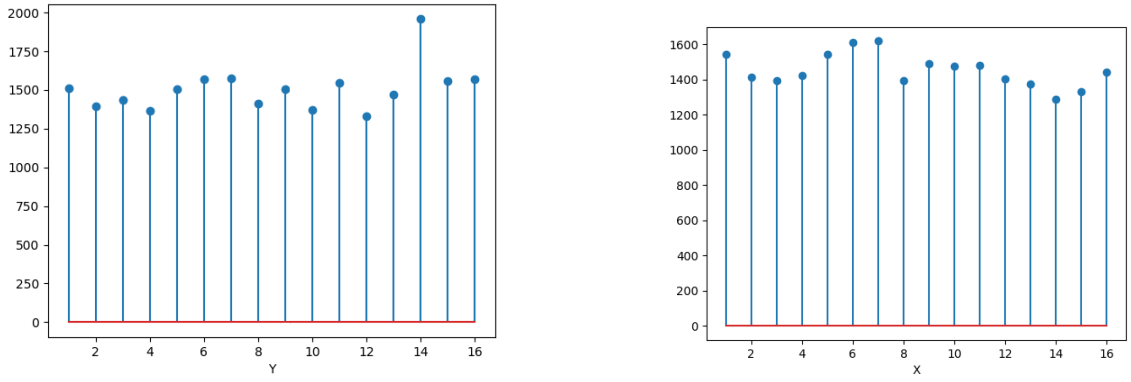

Fig. 13. Counters distribution from cosmic rays

SUMMARY

The amplitude distribution has shown the difference about 20% from the average value for most of channels. However, in the X-plane channels 6 and 7 are distinguished, the first one has the lowest value mean = 6.9, and the second one has the highest mean = 18.1 and the highest sigma.
In the Y plane, channels 1 and 2 with low mean value are highlighted.

Tests of data acquisition block showed its following characteristics:

1) The maximum load was 8 kHz.
2) Event processing time was 15 (μs) (see Fig.14.)

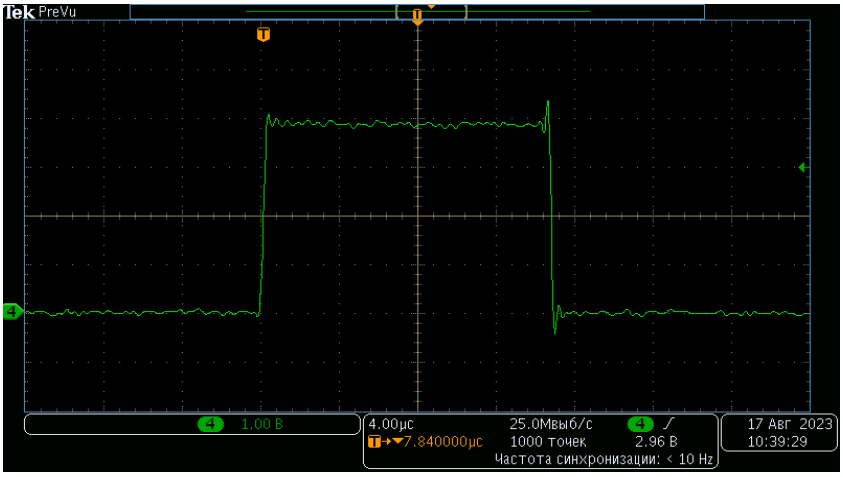

Fig.14. Record prohibition signal, the duration of the signal corresponds to the event processing time.

Fig.15. The experimental setup: 1 - PMT output; 2 - coincidence signal output; 3 - collimator Sr90 β-source; 4 - Microcontroller ATMEGA 328 with USB-connector.

Thus, the work on assembling, setting up and testing a 32-channel scintillation profilometer was completed. Photo of the final installation is shown in (Fig.15) . It is planned to use the installation at the LINAC-200 accelerator for the monitor of the electron beam profile.

REFERENCES

[1] The Theory and Practice of Scintillation Counting: International Series of Monographs in Electronics and Instrumentation

[2] Photon Methods of Radiation Registration is a monograph by Yu. K. Akimov

[3] The control system for the injector of linear accelerator of electrons LINAC-800 is described. The architecture of the control system, structure of equipment and the software are presented. The given system is a part of the ˇrst turn of the control system of electronic accelerator LINAC-800. PACS: 29.20.Ej

[4] e-document: Url:https://www.hamamatsu.com/jp/en/product/optical-sensors/pmt/pmt-assembly/metal-package-type/H8711.html

[5] e-document: Url: https://ww1.microchip.com/downloads/en/DeviceDoc/Atmel-7810-Automotive-Microcontrollers-ATmega328P_Datasheet.pdf

[6] e-document: Url: https://matplotlib.org/stable/index.html

Appendix 1.

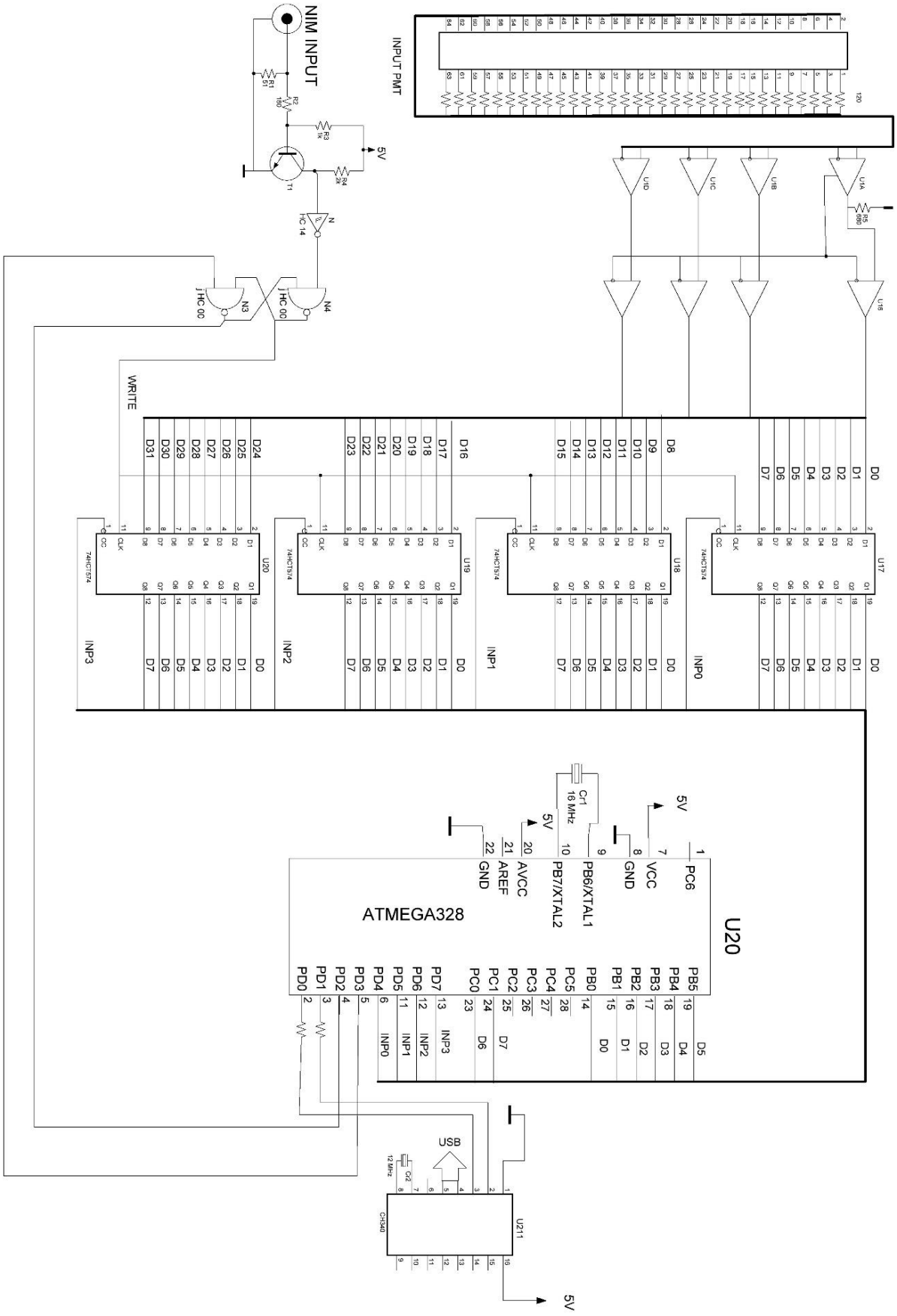
NIM INPUT
INPUT PMT
WRITE
INP0
INP1
INP2
INP3
ATMEGA328
U20
USB
5V
GND
VCC
AVCC
AREF
PB7/XTAL2
PB6/XTAL1
16 MHz
12 MHz
CH340

Appendix 2.

```
#define buffer_SIZE 150    // buffer size
//-------------------------------------------------------
   uint8_t buffer_1[buffer_SIZE];
   uint8_t buffer_2[buffer_SIZE];
   uint8_t buffer_3[buffer_SIZE];  //buffer itself (array)
   uint8_t buffer_4[buffer_SIZE];
   uint32_t time_us[buffer_SIZE];
//-------------------------------------------------------
      uint8_t buffer_head;      // "head" buffer
      uint8_t buffer_tail;      // "tail" buffer
void setup() {
  Serial.begin(2000000);
   pinMode(2, INPUT);//Set pin 2 to input

     DDRB=0;  //Set port B to input
     PORTB=0; //port setting
     DDRC=0;  //Set port C to input
     PORTC=0; //port setting
     DDRD=(1<<7)|(1<<6)|(1<<5)|(1<<4)|(1<<3);//Set port D to
output

    PORTD=0b11110000; //Reset
     delay(10);
    PORTD=0b11111000;
    attachInterrupt(0,overlap, LOW); // interrupt settings
}
void overlap() {
  uint8_t i = (buffer_head + 1 >= buffer_SIZE) ? 0 : buffer_head
+ 1;

       if (i != buffer_tail) {
   time_us[buffer_head]=micros();
       PORTD=0b11101000;//Change the number of the read regis
             delayMicroseconds(2);
             buffer_1[buffer_head]= PINB;

       buffer_1[buffer_head]=buffer_1[buffer_head]+(PINC<<6);

PORTD=0b11011000;//Change the number of the read register
             delayMicroseconds(2);
             buffer_2[buffer_head]=PINB;

       buffer_2[buffer_head]=buffer_2[buffer_head]+(PINC<<6);

PORTD=0b10111000;//Change the number of the read register
             delayMicroseconds(2);
             buffer_3[buffer_head]=PINB;

       buffer_3[buffer_head]=buffer_3[buffer_head]+(PINC<<6);
    PORTD=0b01111000;//Change the number of the read regist
```

```
              delayMicroseconds(2);
              buffer_4[buffer_head]=PINB;

       buffer_4[buffer_head]=buffer_4[buffer_head]+(PINC<<6);

       buffer_head = i;
  }
  PORTD=0b11110000;// reset the trigger
  PORTD=0b11111000;

}
void loop()
{
  if (buffer_head != buffer_tail)
   {

      Serial.print(time_us[buffer_tail]);Serial.print(",");

       Serial.print(buffer_1[buffer_tail],HEX);Serial.print(",");
Serial.print(buffer_2[buffer_tail],HEX);

       Serial.print(",");Serial.print(buffer_3[buffer_tail],HEX);
Serial.print(",");

       Serial.print(buffer_4[buffer_tail],HEX);Serial.println(","
);
       if (++buffer_tail >= buffer_SIZE) buffer_tail = 0;
// "tail" dislocate
 }}
```

Appendix 3.

```
import seaborn as sns
import pandas as pd
import matplotlib.pyplot as plt
from array import array
file = open("Str-90.txt", "r")
data = file.read()
list =data.replace('\n',"").split(",")
file.close()

arr = array('I', [])
x=array("Q",[])
y=array("Q",[])
crdX=array("Q",[0,0,0,0,0,0,0,0,0,0,0,0,0,0,0,0])
crdY=array("Q",[0,0,0,0,0,0,0,0,0,0,0,0,0,0,0,0])
j=1
for i in range(len(list)-1):
    arr.append(eval("0x" + list[i]));
for i in arr:
    print(i);

a=0
while a<len(arr):
    x.append(arr[a]+(256*arr[a+1]))
    a+=4;
b=2
while b<len(arr):
    y.append(arr[b]+(256*arr[b+1]))
    b+=4;
c1=0

while c1<len(x):
    j=0
    while j<16 :
        if (x[c1]>>j) % 2 :
            crdX[j]=crdX[j]+1

        j+=1;
    c1+=1;
c2=0
while c2<len(y):
    p=0
    while p<16 :
        if (y[c2]>>p) % 2 :
            crdY[p]=crdY[p]+1

        p+=1;
    c2+=1;
jk= [1,2,3,4,5,6,7,8,9,10,11,12,13,14,15,16]
plt.figure(1)
plt.stem (jk,crdY)
plt.xlabel("Y")
plt.figure(2)
plt.stem (jk,crdX)
plt.xlabel("X")
plt.show()
```